Supplemental Material can be found at:
http://molpharm.aspetjournals.org/content/suppl/2011/07/08/mol.111.073809.DC1.html

0026-895X/11/8004-630–637$25.00
MOLECULAR PHARMACOLOGY
Vol. 80, No. 4
73809/3716918
Mol Pharmacol 80:630–637, 2011
Printed in U.S.A.
Copyright © 2011 The American Society for Pharmacology and Experimental Therapeutics

Molecular Determinants for Activation of Human *Ether-à-go-go-related* Gene 1 Potassium Channels by 3-Nitro-*N*-(4-phenoxyphenyl) Benzamide[S]

Vivek Garg, Anna Stary-Weinzinger, Frank Sachse, and Michael C. Sanguinetti

Department of Physiology (V.G., M.C.S.), Nora Eccles Harrison Cardiovascular Research & Training Institute (V.G., F.S., M.C.S.), and Department of Bioengineering (F.S.), University of Utah, Salt Lake City, Utah; and Department of Pharmacology and Toxicology, University of Vienna, Vienna, Austria (A.S.-W.)

Received June 2, 2011; accepted July 8, 2011

ABSTRACT

Human *ether-à-go-go-related* gene 1 (hERG1) channels mediate repolarization of cardiac action potentials. Inherited long QT syndrome (LQTS) caused by loss-of-function mutations, or unintended blockade of hERG1 channels by many drugs, can lead to severe arrhythmia and sudden death. Drugs that activate hERG1 are a novel pharmacological approach to treat LQTS. 3-Nitro-n-(4-phenoxyphenyl) benzamide [ICA-105574 (ICA)] has been discovered to activate hERG1 by strong attenuation of pore-type inactivation. Here, we used scanning mutagenesis of hERG1 to identify the molecular determinants of ICA action. Three mutations abolished the activator effects of 30 μM ICA, including L622C in the pore helix, F557L in the S5 segment, and Y652A in the S6 segment. One mutation in S6 (A653M) switched the activity of ICA from an activator to an inhibitor, revealing its partial agonist activity. This was confirmed by showing that the noninactivating mutant hERG1 channel (G628C/S631C) was inhibited by ICA and that the addition of the F557L mutation rendered the channel drug-insensitive. Simulated molecular docking of ICA to homology models of hERG1 corroborated the scanning mutagenesis findings. Together, our findings indicate that ICA is a mixed agonist of hERG1 channels. Activation or inhibition of currents is mediated by the same or overlapping binding site located in the pore module between two adjacent subunits of the homotetrameric channel.

Introduction

The rapid delayed rectifier K^+ current (I_{Kr}) conducted by human *ether-à-go-go-related* gene 1 (hERG1) channels is the predominant repolarizing current of cardiac action potentials in large mammals (Sanguinetti et al., 1995; Trudeau et al., 1995). Slow activation/deactivation and rapid inactivation of hERG1 channels leads to a peak in I_{Kr} during phase 3 repolarization and thus is a critical regulator of action potential duration and heart rate (Sanguinetti and Tristani-Firouzi, 2006). Inherited loss-of-function mutations in hERG1 can induce torsades de pointes (TdP) ventricular arrhythmia (Curran et al., 1995) and accounts for ~40% of all cases of congenital long QT syndromes (LQTS). A gain-of-function mutation in hERG1 has been associated with the rare short QT syndrome (Brugada et al., 2004). Prolonged QT duration and TdP is most commonly an acquired disorder, often caused by block of hERG1 channels as a toxic side effect of several commonly used medications (Sanguinetti and Tristani-Firouzi, 2006). Individuals with either inherited or acquired LQTS are at an increased risk of cardiac arrhythmia and sudden death.

Congenital LQTS is commonly treated by administration of a β-adrenergic receptor blocker, and invasive and costly implantable defibrillators are used for the most severe cases. The available options for short-term drug-induced TdP are intravenous Mg^{2+}, correction of any electrolyte disturbance, and discontin-

This work was supported by the National Institutes of Health National Heart, Lung, and Blood Institute [Grant HL055236]; an American Heart Association (Western States Affiliate) postdoctoral fellowship; and The Austrian Science Fund [Grant P22395].

Article, publication date, and citation information can be found at http://molpharm.aspetjournals.org.

doi:10.1124/mol.111.073809.

[S] The online version of this article (available at http://molpharm.aspetjournals.org) contains supplemental material.

ABBREVIATIONS: hERG1, human *ether-à-go-go*-related gene 1; I_{test}, current activated by membrane depolarization; I_{tail}, tail current; LQTS, long QT syndrome; ICA, ICA-105574, 3-nitro-*N*-(4-phenoxyphenyl) benzamide; V_t, test potential; WT, wild type; DMSO, dimethyl sulfoxide; PH/SF, pore helix/selectivity filter; TdP, torsades de pointes; P, pore; RPR260243, (3*R*,4*R*)-4-(3-(6-methoxyquinolin-4-yl)-3-oxo-propyl)-1-(3-(2,3,5-trifluorophenyl)-prop-2-ynyl)-piperidine-3-carboxylic acid; PD-118057, 2-{4-[2-(3,4-dichloro-phenyl)-ethyl]-phenylamino}-benzoic acid; MES, 4-morpholine ethanesulfonic acid; MD, molecular dynamics; NS1643, 1,3-bis-(2-hydroxy-5-trifluoromethyl-phenyl)-urea; (±)BayK 8644, 1,4-dihydro-2,6-dimethyl-5-nitro-4-[2-(trifluoromethyl)phenyl]-3-pyridinecarboxylic acid, methyl ester.

Downloaded from molpharm.aspetjournals.org by guest on December 1, 2012

MOL PHARM

MOLECULAR PHARMACOLOGY

uation of the culprit drug. These options are inadequate for many patients and a mechanistic-based approach such as enhancing the cardiac repolarizing currents I_{Kr} or I_{Ks} has been proposed (Goldenberg and Moss, 2008). Several compounds that activate hERG1 channels have been fortuitously discovered during routine off-target screening for channel block (Kang et al., 2005; Zhou et al., 2005; Hansen et al., 2006; Gerlach et al., 2010). The mechanisms of action of hERG1 activators include suppression of pore (P)-type inactivation and slowed deactivation. The putative binding site for two hERG1 activators, (3*R*,4*R*)-4-(3-(6-methoxyquinolin-4-yl)-3-oxo-propyl)-1-(3-(2,3,5-trifluoro-phenyl)-prop-2-ynyl)-piperidine-3-carboxylic acid (RPR260243) (Kang et al., 2005) and 2-{4-[2-(3,4-dichlorophenyl)-ethyl]-phenylamino}-benzoic acid (PD-118057) (Zhou et al., 2005), were described recently. The binding sites are distinct and can intuitively explain the predominant mechanism of action of each specific activator. RPR260243 binds near the intracellular gate of the channel (and close to S4–S5 linker) and markedly slows deactivation while also affecting inactivation by an undefined allosteric mechanism (Perry et al., 2007). PD-118057 binds to a pocket formed by the pore helix of one subunit and nearby S6 residues of an adjacent subunit to modestly attenuate P-type inactivation and increase single channel open probability (P_o) with only minor effects on deactivation (Perry et al., 2009).

Another activator of hERG1, 3-nitro-*N*-(4-phenoxyphenyl) benzamide (ICA-105574) was reported to shorten action potential duration of isolated guinea pig cardiomyocytes in a concentration-dependent manner (Gerlach et al., 2010). At the maximally effective concentration, ICA induced a +180 mV shift in the voltage half-point ($V_{0.5}$) of inactivation, resulting in an increased outward current of 10 to 15 times the basal amplitude at 0 mV and slowed the rate of hERG1 current deactivation by 2-fold (Gerlach et al., 2010). To elucidate the molecular determinants for the effects of ICA, we used scanning mutagenesis of the pore region of hERG1, expression of mutant channels in *Xenopus laevis* oocytes and voltage clamp for functional analysis of mutant channels and determined the effects of ICA on inactivation-impaired hERG1 mutant channels.

Materials and Methods

Channel Mutagenesis and Expression in *X. laevis* Oocytes. *HERG1* (*KCNH2*, isoform 1a), was cloned into the pSP64 oocyte expression vector, and mutations were introduced using the QuikChange mutagenesis kit (Agilent Technologies, Santa Clara, CA). Residues Leu553 to Ile567 in S5, Thr618 to Ser624 in PH, and Cys643 to Ile663 in S6 were mutated to alanine or cysteine (to glycine or valine for alanine residues). For some residues, alternate substitutions were introduced to enhance expression (F557L, L622C, F656T, and A661C). Amino acid substitutions at some residues expressed poorly (His562, Trp568, and Ile655) and were not studied further. cRNA was prepared by in vitro transcription with mMessage mMachine SP6 kit (Ambion, Austin, TX) after linearization of the vector plasmid with EcoR1. The isolation, culture, and injection of oocytes with cRNA were performed as described previously (Goldin, 1991; Stühmer, 1992).

Voltage Clamp. Whole-cell hERG1 currents were recorded from oocytes 1 to 4 days after cRNA injection by using the two-microelectrode voltage-clamp technique (Stühmer, 1992). Agarose-tipped microelectrodes (Schreibmayer et al., 1994) were fabricated by filling the tips of 1-mm o.d. borosilicate pipettes with 1% agarose dissolved in 3 M KCl and then back-filling with 3 M KCl. Oocytes were voltage-clamped to a holding potential of −100 mV, and 1-s pulses to a test potential (V_t) of 0 mV were applied every 15 s until current magnitude reached a steady-state level. For standard I-V relationship, step currents were elicited with 1-s pulses from −100 to +50 mV in 10-mV increments. Tail currents were measured at −70 mV. For highly inactivated mutant channels, currents were recorded from oocytes bathed in a Na^+-free extracellular solution with $[K^+]_e$ elevated to 104 mM. Step currents were elicited with 1-s pulses to a V_t that ranged from −100 to +40 mV in 10-mV increments. After each test pulse, the membrane was repolarized to −120 mV. Peak tail currents were plotted as a function of V_t measured before and after 30 μM ICA-105574 (ICA). Values were normalized to the peak values of the control currents (at +40 mV), and the data were fitted to a Boltzmann function to determine the half-point of activation ($V_{0.5}$) and the slope factor (k) of the relationship. Other voltage pulse protocols are described under *Results* and in the figure legends.

After the addition of ICA to the bathing solution, 1-s pulses to 0 mV were applied every 30 s until a new steady-state level was achieved or until 10 min. Relevant voltage protocols were then repeated in the presence of drug.

Gating currents of nonconducting G626A hERG1 mutant channels were measured using the cut-open oocyte Vaseline gap method (Bezanilla and Stefani, 1998), with pulse protocols and solutions optimized for characterizing hERG1 gating currents (Piper et al., 2003). The external solution in the top and guard chambers contained 120 mM tetraethylammonium-MES, 2 mM calcium-MES, and 10 mM HEPES, pH 7.4, with MES. The internal solution in the bottom compartment contained 120 mM potassium MES, 2 mM EDTA, and 10 mM HEPES, pH 7.4 with MES. Signals were low pass-filtered at 10 kHz and digitized at 40 kHz. Linear leak and capacitance currents were compensated by analog circuitry and subtracted online by using a p/−8 [pulse/number (P/N)] protocol.

Single hERG1 channel currents were measured in cell-attached patches as described previously (Zou et al., 1997) using standard techniques (Hamill et al., 1981) and an Axopatch 200B amplifier (Molecular Devices, Sunnyvale, CA). Electrode resistance was 8 to 12 MΩ when pipettes were filled with a solution containing 104 mM potassium gluconate, 2 mM $MgCl_2$, and 10 mM HEPES, pH 7.2 with KOH. The bath solution contained 140 mM KCl, 0.1 mM $CaCl_2$, 2 mM $MgCl_2$, and 10 mM HEPES, pH 7.2 with KOH. Single-channel current amplitudes were determined from analysis of all points amplitude histograms (pCLAMP 9; Molecular Devices) of currents filtered at 1 kHz and digitized at 5 kHz. Data are expressed as mean ± S.E. (n = number of oocytes) and analyzed by the Student's t test.

Molecular Modeling. The homology model of the closed-channel conformation was generated with Modeller 9v7 using the KcsA crystal structure (Protein Data Bank ID 2HVK) as a template. Modeling details, including coordinates for the open conformation, have been described previously (Stary et al., 2010).

Mutants F557L, L622C, Y652A, and A653M of hERG1 were generated in PyMOL (http://www.pymol.org/). MD simulations of closed models were performed with Gromacs version 4.5.4 (http://www.gromacs.org/) (Hess et al., 2008). Wild-type (WT) and mutant channels were embedded in an equilibrated simulation box of palmitoyloleoyl phosphatidylcholine lipids. Lipid parameters were taken from Berger et al. (1997), and the OPLS-all-atom force field (Jorgensen et al., 1996) was used for the protein. The solvent was described by the TIP4P water model (Jorgensen et al., 1983). Electrostatic interactions were calculated explicitly at a distance <1 nm, long-range electrostatic interactions were calculated at every step by particle-mesh Ewald summation (Darden et al., 1993). Lennard-Jones interactions were calculated with a cutoff of 1 nm. All bonds were constrained by using the LINCS algorithm (Hess et al., 1997), allowing for an integration time step of 2 fs. The Nose-Hoover thermostat (Nose, 1984) was used for temperature coupling (τ = 0.1 ps) and the Parrinello-Rahman barostat algorithm (Parrinello and Rahman, 1981) for pressure coupling. Conjugate gradient energy-minimization steps (1000) were performed, followed by 2 ns of re-

Downloaded from molpharm.aspetjournals.org by guest on December 1, 2012

strained MD, in which the protein atoms were restrained with a force constant of 1000 kJ/mol^{-1} · nm^{-2} to their initial position, whereas ions, lipids, and solvent were allowed to move freely. Each system was then subjected to 2 × 10 ns of unrestrained MD, during which coordinates were saved every 1 ps for analysis.

Coordinates of ICA105574 were generated with GaussView 5, and the geometry was optimized with the Hartee-Fock 3–21G basis set implemented in Gaussian 09 (Gaussian Inc., Wallingford, CT) (Frisch et al., 2009). Docking was performed with the program Gold 4.0.1 (Jones et al., 1995). Coordinates of the geometric center calculated among residues Phe557, Leu622, Tyr652, and Ala653 were taken as binding site origin. The binding site radius was set equal to 10 Å. Operations (150,000) of the GOLD genetic algorithm were used to dock the selected compounds into the WT and mutant channels. Three snapshots (3, 6, and 8 ns) were taken from MD trajectories. The Chemscore scoring function was used to estimate free energies of binding (Gold.Chemscore.DG). Reported values are averaged over the 10 best docking poses.

Solutions and Drugs. For two-microelectrode voltage-clamp experiments, the extracellular solution contained the following: 98 mM NaCl, 2 mM KCl, 1 mM $CaCl_2$, 1 mM $MgCl_2$, and 5 mM HEPES, pH 7.6. ICA was purchased from Sigma-Aldrich (St. Louis, MO). Drug solutions were prepared fresh just before experiment by dilution of a 10 mM DMSO stock solution of ICA. Each oocyte was treated with a single concentration (30 μM) of drug unless specified otherwise.

Results

ICA Increases hERG1 Current by Suppressing Inactivation But Has No Effect on Single-Channel Conductance, Maximal Conductance, or Gating Currents. The effects of 10 and 30 μM ICA on WT hERG1 channels expressed in *X. laevis* oocytes are illustrated in Fig. 1, A and B. ICA induced a marked concentration-dependent enhancement of current magnitude. Activation of hERG1 current by 30 μM ICA reached a steady state in ~10 min at 30 μM. The fold increase in current assayed with 1-s pulses to a test potential (V_t) of +20 mV was 7.6 ± 1.1 at 10 μM and 28 ± 3.4 at 30 μM, (n = 3–8). The potency of ICA was reduced in

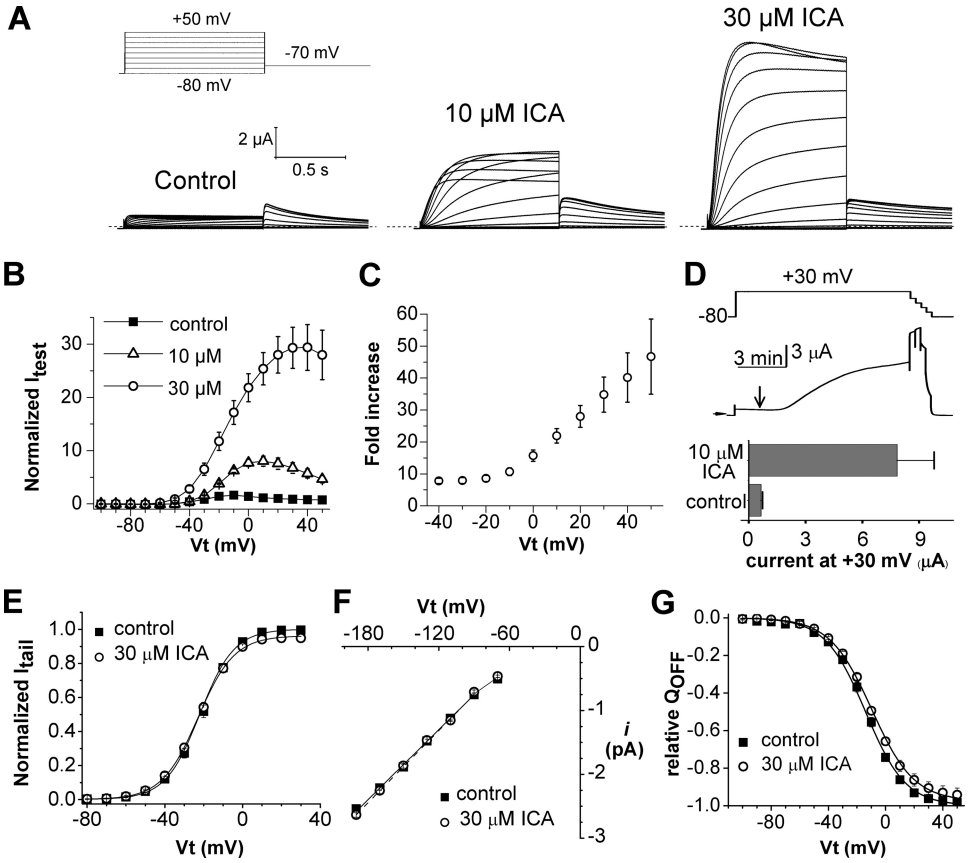

Fig. 1. Voltage-dependent activation of hERG1 current by ICA-105574 (ICA) in *X. laevis* oocytes. A, ICA increases the magnitude of hERG1 current. Currents were elicited with 1-s pulses to test potentials applied in 10-mV increments from −80 to +50 mV. Tail currents (I_{tail}) were measured at −70 mV. Voltage protocol is shown above control current traces. B, I-V_t relationships measured before (control) and in presence of 10 and 30 μM ICA (n = 3–8). Currents were normalized relative to the peak outward control current at +20 mV. C, fold increase in normalized peak outward current induced by 30 μM ICA plotted as a function of V_t (n = 8). D, ICA binds to open/inactivated state of hERG1 channels. Top, voltage-clamp protocol. Middle, corresponding current trace showing time of application of 10 μM ICA (arrow). After several minutes at +30 mV, the voltage was progressively stepped down from 0 to −80 mV in 20-mV increments. Bottom, plot of current magnitude at +30 mV before (control) and after 10 min in the presence of 10 μM ICA (n = 4). E, plot of peak I_{tail} versus V_t determined before and after 30 μM ICA in oocytes bathed in 104 mM $[K^+]_e$ solution. Currents were activated with 1-s pulses to a variable V_t and I_{tail} was measured at −140 mV. Peak I_{tail} magnitude was determined by fitting the current decay to a biexponential function and extrapolating the fit to the onset of membrane repolarization then normalized relative to the peak of control I_{tail} for each oocyte. Data were fitted with a Boltzmann function (smooth curves). For control, $V_{0.5}$ = −22 ± 0.5 mV, k = 8.8 ± 0.3 mV; for ICA, $V_{0.5}$ = −22.9 ± 0.3 mV, k = 9.3 ± 0.2 mV (n = 9). F, single-channel I-V_t relationship determined for cell-attached patches from oocytes bathed in control or 30 μM ICA solution. Slope conductance determined by linear fit of data for the V_t range of −100 to −180 mV was 18.1 ± 0.39 pS (n = 10) in control patches and 18.6 ± 0.28 pS (n = 10) in the presence of 30 μM ICA. G, ICA does not alter the voltage-dependence or maximal value of charge displacement ($Q_{OFF-max}$) associated with the OFF gating current of hERG1 channels. Normalized $Q_{OFF-max}$ was plotted as a function of V_t and fitted with a Boltzmann function (smooth curves). For control, $V_{0.5}$ = −14.0 ± 0.6 mV, k = 14.1 ± 0.3 mV; for ICA, $V_{0.5}$ = −9.7 ± 0.1 mV, k = 14.7 ± 0.3 mV (n = 9). The slight shift in $V_{0.5}$ was also observed for vehicle (DMSO) control (see Supplemental Fig. 1).

Downloaded from molpharm.aspetjournals.org by guest on December 1, 2012

MOL PHARM
MOLECULAR PHARMACOLOGY
aspet

oocytes compared with that reported (Gerlach et al., 2010) for human embryonic kidney 293 cells (EC_{50} = 0.5 μM), probably because ICA is highly lipophilic (logP = 3.69) and accumulates in the yolk of oocytes (Witchel et al., 2002). The increase in current by ICA was associated with a marked decrease in rectification of the current-voltage ($I\text{-}V_t$) relationship (Fig. 1B) and an enhanced effect at more positive test potentials (Fig. 1C), effects consistent with a large drug-induced positive shift in the $V_{0.5}$ of inactivation as reported previously (Gerlach et al., 2010). ICA binds to the closed state of the hERG1 channel (Gerlach et al., 2010). In Fig. 1D, we show that ICA can also bind to channels when applied to an oocyte during a prolonged depolarizing step to +30 mV, indicating that the drug can also bind to channels in the open or inactivated state.

The voltage-dependence of the hERG1 channel conductance-voltage relationship was determined by measuring peak tail currents (I_{tail}) after a 1-s depolarizing pulse to a variable V_t. For these experiments, oocytes were bathed in 20 mM $[K^+]_o$ solution to preclude variation in I_{tail} magnitude caused by the transient local accumulation of extracellular K^+ and thus, chemical driving force associated with large outward currents and low $[K^+]_o$. When I_{tail} values were elicited at −140 mV, a potential in which recovery from inactivation is rapid and complete, ICA did not alter the voltage-dependence or G_{max} of the conductance-voltage relationship for hERG1 (Fig. 1E). This finding suggests that ICA does not cause any significant change in single-channel activity or induce recruitment of channels to the surface membrane. To confirm these expectations, we determined the effect of ICA on single-channel conductance and gating currents.

Single hERG1 channel activity was determined in cell-attached patches of oocytes using pipettes filled with 104 mM $[K^+]_o$ solution (Supplemental Fig. 1). The slope conductance for single-channel activity was not altered when 30 μM ICA was included in the pipette and bath solution (Fig. 1F). Although unlikely, ICA might also increase current magnitude by recruiting channels from a cytoplasmic store to the plasma membrane. As an indirect measure of plasma-membrane bound channel density, we determined the maximum intramembrane charge displacement ($Q_{OFF\text{-}max}$) associated with the OFF gating current. The cut-open oocyte voltage-clamp technique (Stefani and Bezanilla, 1998) was used to measure hERG1 gating currents. ICA had no effect on the kinetics of gating currents or the magnitude of the maximum intramembrane charge displacement ($Q_{OFF\text{-}max}$) associated with the OFF gating current compared with currents treated with vehicle (DMSO) (Fig. 1G and Supplemental Fig. 1). Together, these findings indicate that the ICA-induced increase in hERG1 current is not due to an increase in maximum whole-cell conductance, single-channel conductance, or an increased number of functional channels at the surface membrane and, thus, can be attributed solely to a marked attenuation of P-type inactivation (Gerlach et al., 2010).

To further explore the role of inactivation in the mechanism of action of ICA, its effects on three inactivation-impaired mutant hERG1 channels were determined (Fig. 2). S620T hERG1 channels have greatly reduced inactivation (Ficker et al., 1998) and, as expected, exhibited a greatly reduced response to ICA (only 1.3 ± 0.2-fold increase at +50 mV, n = 7). Two other point mutations (S631A, N588K) also attenuate hERG1 inactivation (Schönherr and Heinemann, 1996; Brugada et al., 2004), albeit to a lesser extent than the S620T mutation, and as expected, these channels were more sensitive to the drug compared with S620T hERG1 channels (Fig. 2). At +50 mV, 30 μM ICA increased S631A channel currents by 3.2 ± 0.2-fold (n = 4) and N588K channel currents by 2.4 ± 0.1-fold (n = 3), far less that the 47-fold enhancement observed for WT hERG1 channels (Fig. 1C). Thus, current enhancement by ICA is strongly correlated with the extent of intrinsic P-type inactivation of hERG1 channels.

Molecular Determinants for ICA Binding. Based on mutational analysis of hERG1 (Ficker et al., 1998), the entire pore module, including the pore helix/selectivity filter (PH/SF), S5 and S6 segments participate in channel inactivation.

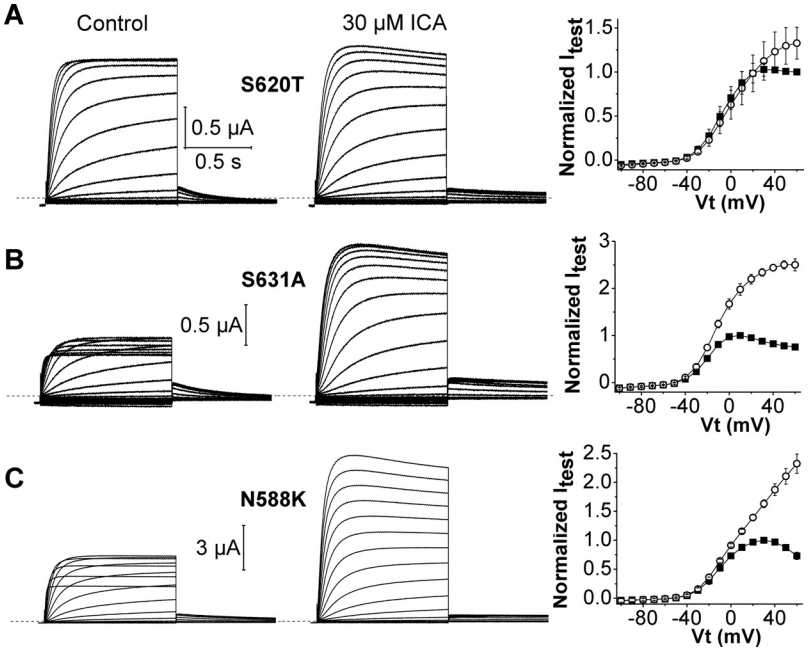

Fig. 2. Mutant channels with impaired inactivation are less sensitive to ICA. A, S620T hERG1 currents recorded before (control) and after 30 μM ICA (left and middle). Currents were elicited as described in Fig. 1A. Right, plots of mean $I\text{-}V_t$ relationships determined before (■) and after 30 μM ICA (○). Currents (I_{test}) were measured at the end of 1-s test pulses and normalized relative to the peak outward value of control currents (n = 7). B and C, current traces (left and middle) and $I\text{-}V_t$ relationships (right) for S631A (n = 4) and N558K (n = 3) hERG1 channels.

Downloaded from molpharm.aspetjournals.org by guest on December 1, 2012

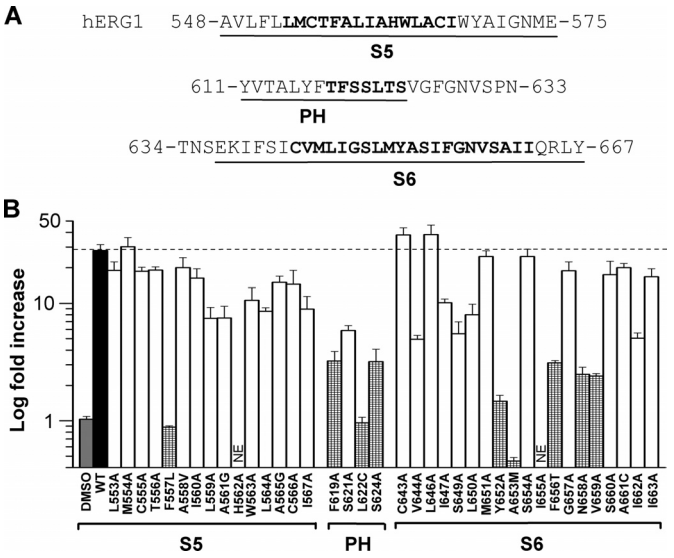

Fig. 3. Molecular determinants of hERG1 channel sensitivity to ICA. A, sequence of the S5 and pore helix-S6 domains of a hERG1 subunit. The S5, pore helix, and S6 segments are underlined, and the scanned residues are indicated by boldface text. B, bar graph summarizing fold increase in hERG1 current magnitude at +20 mV induced by 30 μM ICA for WT (■) or channels containing single point mutations as indicated. High-impact residues (≥10-fold reduction in drug effect compared with WT hERG1, $p < 0.0005$) are indicated by checkered bars. Vehicle control (DMSO) had no effect. NE, no functional expression.

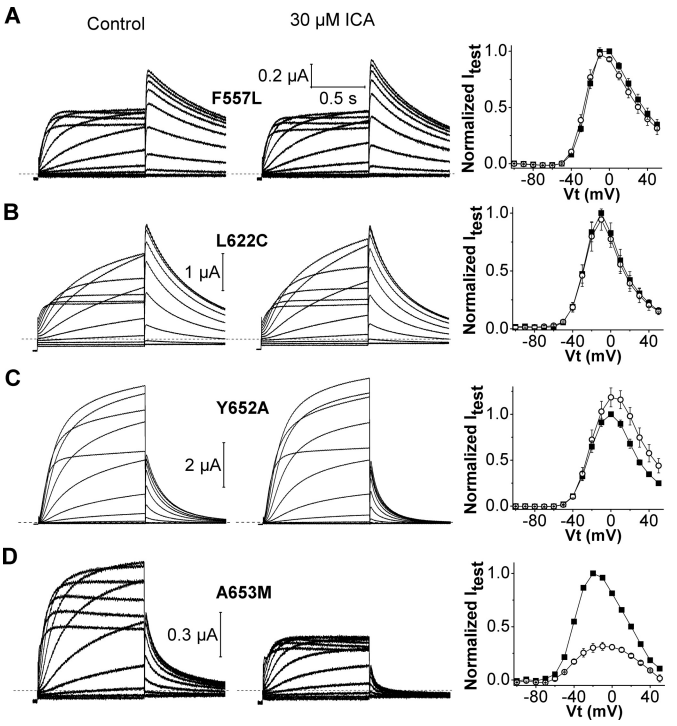

Fig. 4. Mutation of Phe557, Leu622, Tyr652, or Ala653 eliminates or reverses agonist activity of ICA on hERG1. A, left and middle, F557L hERG1 currents (elicited as described in Fig. 1A) recorded before (control) and after 30 μM ICA. Right, I-V_t relationships for currents at the end of 1-s test pulse determined before (■) and after treatment of cells with 30 μM ICA (○). Currents were normalized relative to peak outward value of control current. B to D, current traces (left and middle) and I-V_t relationships (right) for L622C (B), Y652A (C), and A653M (D) hERG1 channels.

To determine the molecular determinants of ICA activity, we performed scanning mutagenesis of major portions of the hERG1 pore module (Fig. 3A). A total of 44 residues were mutated, including Leu553 to Ile567 in S5, Thr618 to Ser624 in the PH/SF, and Cys643 to Ile663 in S6. The effect of ICA (30 μM for 10 min) on individual mutant channels was quantified as the fold increase in outward current measured at the end of a 1-s pulse to a V_t of +20 mV (Fig. 3B).

Nine mutations attenuated the response to 30 μM ICA by ≥10-fold and were classified as "high impact" residues (Fig. 3B). All of these mutant channels exhibited normal P-type inactivation as revealed by their typical bell-shaped I-V_t relationships. Three mutations prevented the activation of hERG1 by ICA. F557L and L622C channels were completely insensitive to 30 μM ICA (Fig. 4, A and B). ICA induced a slight but insignificant increase in outward Y652A channel currents and accelerated the rate of current deactivation; at −70 mV, the time constants for fast and slow phases of deactivation (τ_f and τ_s) were 99 ± 9.8 and 329 ± 36 ms for control, respectively, compared with 53 ± 8.3 and 221 ± 37 ms for 30 μM ICA ($n = 6$). Currents at +20 mV for five other mutant channels (F619A, S624A, F656T, N658A, and V659A) were increased <3-fold by 30 μM ICA (Supplemental Fig. 2). ICA inhibited one mutant hERG1 channel (A653M) and accelerated its rate of deactivation (Fig. 4D); at −70 mV, τ_f and τ_s were 60 ± 3.9 and 283 ± 25 ms for control, respectively, compared with 41 ± 3.7 and 216 ± 27 ms for drug ($n = 6$). In contrast to Y652A and A653M channels, ICA slowed the rate of monoexponential deactivation of WT channels at −70 mV by ~2-fold, from 413 ± 10 to 751 ± 62 ms ($n = 6$). Four mutant channels (T618A, T623A, M645C, and G648A) exhibited enhanced inactivation or very low expression and were therefore recorded in an extracellular solution containing 104 mM K^+ to accentuate the magnitude of inward I_{tail}. ICA enhanced T618A channel currents, but reduced T623A, M645C, and G648A channel currents by 30 to 50% (Supplemental Fig. 3). In summary, scanning mutagenesis identified three mutations (F557L, L622C, Y652A) that eliminated or attenuated the activator effects as well as four mutations (T623A, M645C, G648A, and A653M) that revealed an inhibitory activity of ICA.

Phe557, Leu622, and Tyr652 are likely key components of the binding site for ICA because both activator and inhibitory effects were prevented by mutation of these residues. Thr623, Ser624, Met645, Gly648, Tyr652, Phe656, and Val659 line the internal cavity, and some of these residues are important molecular determinants for pore block by hERG1 channel inhibitors (Mitcheson et al., 2000). Several of the high-impact residues identified here for ICA were found previously to be important for other hERG1 activators, including RPR260243 (Phe557, Tyr652, Asn658, and Val659) (Perry et al., 2007) and PD-118057 (Phe619, Leu622, and Met645) (Perry et al., 2009). Thus, the molecular determinants of channel activation by ICA overlap, but are not identical with other well characterized hERG1 activators and blockers.

Simulated Docking of ICA on hERG1. A homology model of the hERG1 pore module was constructed by using the KcsA (closed state) and KvAP (open state) channel structures as templates. ICA binds perpendicularly to the channel axis between two adjacent subunits of the pore module in both the open (Fig. 5A) and closed (Fig. 5C) states. A close-up view of the putative drug-binding region is depicted in Fig. 5, B and D, in which the high-impact residues identified by scanning mutagenesis and a few other residues in close con-

MOL PHARM
MOLECULAR PHARMACOLOGY
aspet
Downloaded from molpharm.aspetjournals.org by guest on December 1, 2012

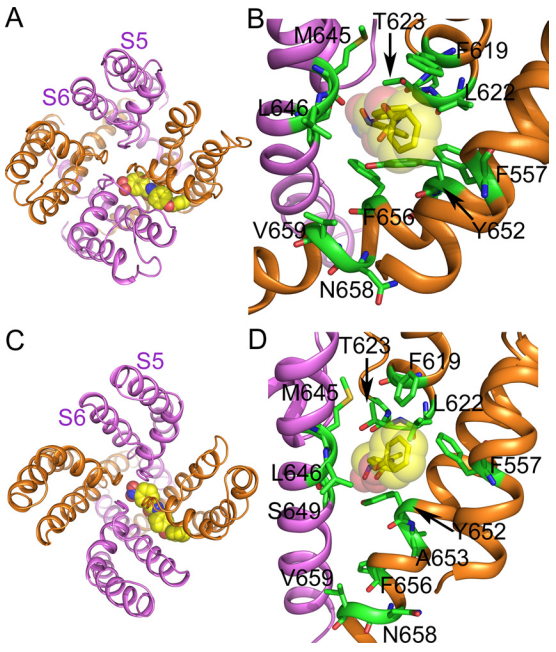

Fig. 5. ICA docked to a KvAP- (open-state) and KcsA- (closed-state) based homology model of the hERG1 pore module. A, open-state pore module of the channel (ribbons) as viewed from the extracellular space. ICA is shown in space fill. B, close-up view of the putative drug-binding region to the open-state channel. Residues designated as high-impact based on scanning mutagenesis using low $[K^+]_e$ solution (Phe557, Phe619, Leu622, Ser624, Tyr652, Ala653, Phe656, Val659, and Asn658) or high $[K^+]_e$ solution (Thr623, Met645) are labeled and are shown as stick models. Also labeled is one additional residue (Leu646) predicted to be in close contact with drug that exhibited a normal drug response when mutated to alanine. C, ICA binding to the closed-state pore module of the channel as viewed from the extracellular space. D, close-up view of the putative drug-binding region with labeling the same as in B.

tact with the drug are shown in stick mode. Except for Val659 and Asn658, all high-impact residues from the scanning mutagenesis are in close contact with ICA. In both the open and closed states of the channel, ICA resides in a hydrophobic pocket formed by Leu622, Phe619, Phe557, Tyr652, and Phe656. ICA interacts with Phe619, Phe557, and Tyr652 via π-π stacking and stabilizes the Tyr652 side chain in the down conformation (toward the cytoplasmic side of channel), in agreement with previous MD simulations (Zachariae et al., 2009). In addition, hydrogen bonds are (frequently) predicted between ICA and the backbone of Leu622, the side chain and/or backbone of Ser624, Thr623, and Ser649 (Supplemental Fig. 4, A and B).

The predicted binding mode of ICA is altered by the mutations that eliminated the activator effects of ICA (Supplemental Figs. 4 and 5). Atomistic molecular dynamics simulations revealed conformational changes in hERG1. For example, the F557L mutation induced side chain rotations of several residues (Leu646, Phe619, Leu622, and Thr623) that reduce the size of the lipophilic pocket. In F557L and L622C mutant channels, ICA bound to the outside of the pore module. A653M allosterically reorients the side chains of Phe619, Leu622, and Phe557, removing the lipophilic pocket. In addition, in A653M channels, hydrogen bonds to Tyr652 and Ser649 (in S6) and Ser624 and Thr623 (selectivity filter) are frequently predicted by GOLD, and in contrast to WT channels, the Tyr652 side chain frequently adopts an up-conformation. The Chemscore scoring function was used to estimate free energies of binding (Gold.Chemscore.DG) of ICA and were averaged over the 10 best docking poses for WT and mutant channels. ΔG values were −40.9 and −40.54 kJ/mol for WT channels in the closed and open states, respectively, and were reduced in the closed state of the mutant channels as follows: −32.97 (F557L), −36.09 (L622C), −37.69 (Y652A), and −38.21 kJ/mol (A653M).

A Single Residue in S5 of hERG1 Determines whether ICA Is an Activator or Inhibitor. We next determined the effects of ICA on a mutant hERG1 channel that does not inactivate. Combined mutation of two residues (G628C/S631C) located near or within the selectivity filter of hERG1 completely removes channel inactivation and reduces K^+ selectivity (Smith et al., 1996). Currents conducted by G628C/S631C hERG1 channels were not augmented by ICA; instead, a 30 μM concentration of the drug decreased currents by 40% (Fig. 6, A and B). This reduction of current could result from drug binding to the central cavity receptor described for potent hERG1 blockers (Mitcheson et al., 2000). An important component of the blocker binding site is Tyr652, and mutations of this residue can greatly attenuate drug-induced block of WT channels. However, introduction of the Y652A mutation did not alter the response of G628C/S631C hERG1 channels to ICA (Fig. 6C), suggesting that current reduction is not caused by binding of ICA to the central cavity. Moreover, introduction of the F557L mutation (that prevents activator effects on WT channels) eliminated the response of G628C/S631C hERG1 channels to ICA (Fig. 6D). Together these findings suggest that ICA exerts its

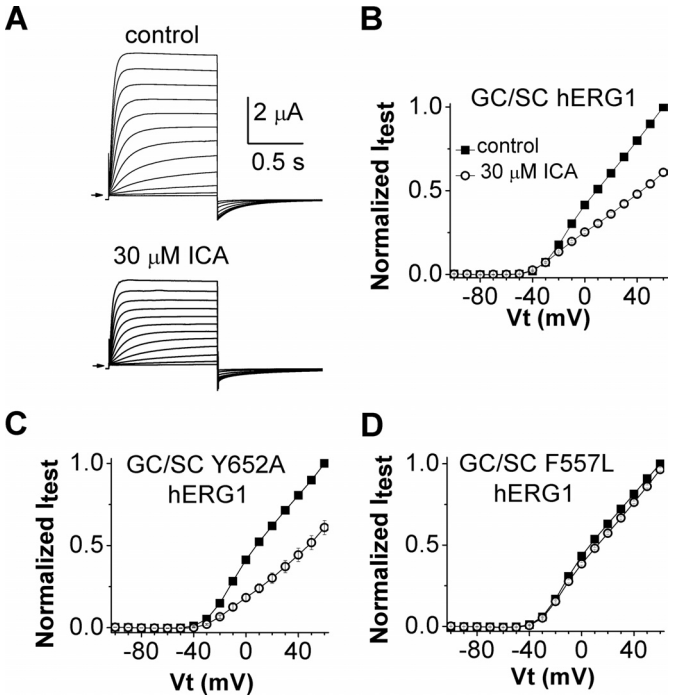

Fig. 6. Mutation of phenylalanine to leucine in S5 eliminates the inhibitory effect of ICA in a noninactivating mutant hERG1 channel. A, ICA inhibits noninactivating G628C/S631C (GC/SC) hERG1 mutant channels. Currents were elicited as described in Fig. 1A and were recorded before (control) and after 10 min of 30 μM ICA. B, I-V_t relationships for currents measured at the end of 1-s test pulses before (■) and after treatment of cells with 30 μM ICA (○). Currents were normalized relative to control current at +60 mV (n = 6). C, Y652A/G628C/S631C hERG1 channels are also blocked by 30 μM ICA (○) (n = 8). D, F557L/G628C/S631C hERG1 channels are insensitive to 30 μM ICA (○) (n = 12).

Downloaded from molpharm.aspetjournals.org by guest on December 1, 2012

MOL PHARM
MOLECULAR PHARMACOLOGY
aspet

agonist and antagonist effects by binding to a single or overlapping receptor site.

Discussion

Activation of hERG1 channels by ICA is state-independent and mediated by a pronounced positive shift in the voltage dependence of P-type inactivation (Gerlach et al., 2010). P-type inactivation is caused by very subtle changes in the dynamic structure of the selectivity filter (Cuello et al., 2010b). Mutation of residues located within or near the PH/SF that impaired inactivation (S620T, S631A) caused reduced sensitivity to the drug. Inhibition of a mutant channel (G628C/S631C hERG1) with inactivation removed (Smith et al., 1996) revealed that ICA also has intrinsic antagonist activity. Phe557 (S5) and Leu622 (PH) are considered to be the most critical determinants of the binding site because single mutations of either residue prevented drug-induced changes in current magnitude and kinetics.

Voltage-gated channels can be considered analogous to intrinsically active receptors that are modulated by voltage. Viewed in this manner, ICA can behave as either an agonist or an inverse agonist of hERG1 channels. The drug is an agonist (i.e., activator) when bound to WT hERG1 channels and an inverse agonist (i.e., inhibitor) when bound to A653M or G628C/S631C hERG1 channels. Strictly speaking, the term inverse agonist would apply only if ICA bound to the same site to mediate both activator and inhibitory effects. Inhibition of noninactivating mutant hERG1 channels could simply result from pore block, mediated by binding of ICA to the central cavity as described for a plethora of hERG1 blockers (Mitcheson et al., 2000; Sanguinetti and Mitcheson, 2005) and distinct from the proposed activator site. Alternatively, both activation and inhibition of channel activity by ICA could arise from its binding to a single site as proposed for dihydropyridines that can either activate or inhibit L-type Ca^{2+} channels (Hockerman et al., 1997). For several reasons, we favor the hypothesis that ICA binds to a single site in both WT or mutant channels, and that current inhibition results from stabilization of channels in a closed (or inactivated) state rather than pore blockage per se. First, the putative activator site described for WT channels should remain intact in G628C/S631C hERG1 channels; lack of drug effect on F557L/G628C/S631C hERG1 channels supports this view. Second, if ICA bound to the well characterized central cavity site (Mitcheson et al., 2000), mutation of Tyr652 or Phe656 in hERG1 would be expected to cause an enhanced activator response rather than the observed diminished response. The side chains of these aromatic residues are the most important molecular determinants of many hERG1 blockers (Sanguinetti and Mitcheson, 2005). Mutation of Phe656 to threonine enhanced the activator effect of 1,3-bis-(2-hydroxy-5-trifluoromethyl-phenyl)-urea (NS1643) compared with WT channels (Casis et al., 2006), consistent with two binding sites for this compound: one that mediates activation, and another (in the central cavity) that mediates pore block. In contrast, F656T channels were less sensitive to ICA. Third, a conserved phenylalanine in S5 was a key determinant of both activator and inhibitory effects of ICA in hERG1 channels. Mutation of Phe557 to leucine in hERG1 (F557L) eliminated all effects of the drug. Finally, A653M hERG1 channels exhibit normal inactivation, but currents were inhibited, and deactivation was accelerated by the drug. Modeling suggests that the A653M mutation reverses the orientation of the side chain of Tyr652 (from a down to an up configuration); perhaps this interferes with the coupling between drug binding and altered inactivation gating. Whatever the underlying mechanisms, A653M in hERG1 reveals an intrinsic antagonist activity of ICA that is normally masked by its dominant activator effect. A similar switch from agonist to antagonist activity was reported for 1,4-dihydro-2,6-dimethyl-5-nitro-4-[2-(trifluoromethyl)phenyl]-3-pyridinecarboxylic acid, methyl ester [(±)BayK 8644] after mutation of two adjacent residues (Tyr1485, Met1486) in domain IV S6 of the α_{1c} L-type calcium channel (Schuster et al., 1996). It is noteworthy that the topology of the putative ICA binding site, a hydrophobic pocket located between two adjacent subunits of the pore module, is similar to the proposed dihydropyridine binding site in L-type calcium channels (Cosconati et al., 2007; Tikhonov and Zhorov, 2009) and the binding site for brevetoxins and ciguatoxin (neurotoxin receptor site 5) in voltage-gated sodium channels (Catterall et al., 2007). All of these lipophilic compounds alter channel gating and are proposed to gain direct access to the pore module via the lipid membrane.

Mutation of Tyr652 to alanine prevents the attenuation of inactivation normally caused by RPR260243 (Perry et al., 2007). However, deactivation of Y652A hERG1 channels is markedly slowed by RPR260243 (Perry et al., 2007), indicating that the mutation does not prevent drug binding. Y652A channels are also resistant to the normally pronounced effect of ICA on inactivation. However, opposite to the effects on WT channels, deactivation of Y652A channels was accelerated by ICA. The ability of both ICA and RPR260243 to affect deactivation but not inactivation of Y652A channels suggests that Tyr652 residues are required for coupling drug binding to suppression of channel inactivation. Modeling suggests that Tyr652 directly interacts with ICA but not with RPR260243 (Perry et al., 2007). Based on sequence alignments of S6 segments, Tyr652 is equivalent to Phe103 of KcsA and Ile470 of Shaker K^+ channels. Mutation of Phe103 (KcSA channel) or Ile470 (Shaker channel) drastically suppresses C-type inactivation, and Cuello et al. (2010a) have proposed that these key residues in S6 allosterically couple the cytosolic gate with the extracellular gate (selectivity filter), so-called bidirectional coupling. In contrast, mutations of Tyr652 in hERG1 do not appreciably alter inactivation gating (Fernandez et al., 2004). The mechanism responsible for disrupted coupling between drug binding and altered inactivation of Y652A hERG1 channels requires further study.

In summary, ICA binds to a hydrophobic pocket located between two adjacent hERG1 channel subunits, resulting in a subtle change in configuration of the selectivity filter that disrupts inactivation gating. Binding of ICA to the same or overlapping site mediates inhibition of mutant A653M and G628C/S631C hERG1 channels.

Acknowledgments

We thank Jennifer Abbruzzese for measurement of gating currents, Tobias Linder and Kirsten Knape for help with modeling figures, and Kam Hoe Ng for isolation and injection of oocytes.

MOL PHARM
MOLECULAR PHARMACOLOGY
aspet
Downloaded from molpharm.aspetjournals.org by guest on December 1, 2012

MOL PHARM

MOLECULAR PHARMACOLOGY

Authorship Contributions

Participated in research design: Garg and Sanguinetti.

Conducted experiments: Garg and Sanguinetti.

Performed data analysis: Garg, Stary-Weinzinger, Sachse, and Sanguinetti.

Wrote or contributed to the writing of the manuscript: Garg, Stary-Weinzinger, and Sanguinetti.

References

Berger O, Edholm O, and Jähnig F (1997) Molecular dynamics simulations of a fluid bilayer of dipalmitoylphosphatidylcholine at full hydration, constant pressure, and constant temperature. *Biophys J* **72:**2002–2013.

Bezanilla F and Stefani E (1998) Gating currents. *Methods Enzymol* **293:**331–352.

Brugada R, Hong K, Dumaine R, Cordeiro J, Gaita F, Borggrefe M, Menendez TM, Brugada J, Pollevick GD, Wolpert C, et al. (2004) Sudden death associated with short-QT syndrome linked to mutations in HERG. *Circulation* **109:**30–35.

Casis O, Olesen SP, and Sanguinetti MC (2006) Mechanism of action of a novel human ether-a-go-go-related gene channel activator. *Mol Pharmacol* **69:**658–665.

Catterall WA, Cestèle S, Yarov-Yarovoy V, Yu FH, Konoki K, and Scheuer T (2007) Voltage-gated ion channels and gating modifier toxins. *Toxicon* **49:**124–141.

Cosconati S, Marinelli L, Lavecchia A, and Novellino E (2007) Characterizing the 1,4-dihydropyridines binding interactions in the L-type Ca^{2+} channel: model construction and docking calculations. *J Med Chem* **50:**1504–1513.

Cuello LG, Jogini V, Cortes DM, Pan AC, Gagnon DG, Dalmas O, Cordero-Morales JF, Chakrapani S, Roux B, and Perozo E (2010a) Structural basis for the coupling between activation and inactivation gates in K^+ channels. *Nature* **466:**272–275.

Cuello LG, Jogini V, Cortes DM, and Perozo E (2010b) Structural mechanism of C-type inactivation in K^+ channels. *Nature* **466:**203–208.

Curran ME, Splawski I, Timothy KW, Vincent GM, Green ED, and Keating MT (1995) A molecular basis for cardiac arrhythmia: *HERG* mutations cause long QT syndrome. *Cell* **80:**795–803.

Darden T, York D, and Pedersen L (1993) Particle mesh Ewald: An N [center-dot] log(N) method for Ewald sums in large systems. *J Chem Phys* **98:**10089–10092.

Fernandez D, Ghanta A, Kauffman GW, and Sanguinetti MC (2004) Physicochemical features of the HERG channel drug binding site. *J Biol Chem* **279:**10120–10127.

Ficker E, Jarolimek W, Kiehn J, Baumann A, and Brown AM (1998) Molecular determinants of dofetilide block of HERG K^+ channels. *Circ Res* **82:**386–395.

Frisch MJ, Trucks GW, Schlegel HB, Scuseria GE, Robb MA, Cheeseman JR and Scalmani G (2009) Gaussian 09, Revision A. 1 Gaussian, Inc., Wallingford.

Gerlach AC, Stoehr SJ, and Castle NA (2010) Pharmacological removal of human ether-à-go-go-related gene potassium channel inactivation by 3-nitro-N-(4-phenoxyphenyl) benzamide (ICA-105574). *Mol Pharmacol* **77:**58–68.

Goldenberg I and Moss AJ (2008) Long QT syndrome. *J Am Coll Cardiol* **51:**2291–2300.

Goldin AL (1991) Expression of ion channels by injection of mRNA into Xenopus oocytes. *Methods Cell Biol* **36:**487–509.

Hamill OP, Marty A, Neher E, Sakmann B, and Sigworth FJ (1981) Improved patch-clamp techniques for high-resolution current recording from cells and cell-free membrane patches. *Pflugers Arch* **391:**85–100.

Hansen RS, Diness TG, Christ T, Demnitz J, Ravens U, Olesen SP, and Grunnet M (2006) Activation of human ether-a-go-go-related gene potassium channels by the diphenylurea 1,3-bis-(2-hydroxy-5-trifluoromethyl-phenyl)-urea (NS1643). *Mol Pharmacol* **69:**266–277.

Hess B, Bekker H, Berendsen HJC, and Fraaije JG (1997) LINCS: a linear constraint solver for molecular simulations. *J Comput Chem* **18:**1463–1472.

Hess B, Kutzner C, van der Spoel D, and Lindahl E (2008) GROMACS 4: Algorithms for highly efficient, load-balanced, and scalable molecular simulation. *J Chem Theory Comput* **4:**435–447.

Hockerman GH, Peterson BZ, Johnson BD, and Catterall WA (1997) Molecular determinants of drug binding and action on L-type calcium channels. *Annu Rev Pharmacol Toxicol* **37:**361–396.

Jones G, Willett P, and Glen RC (1995) Molecular recognition of receptor sites using a genetic algorithm with a description of desolvation. *J Mol Biol* **245:**43–53.

Jorgensen WL, Chandrasekhar J, Madura JD, Impey RW, and Klein ML (1983) Comparison of simple potential functions for simulating liquid water. *J Chem Phys* **79:**926–935.

Jorgensen WL, Maxwell DS, and Tirado-Rives J (1996) Development and testing of the OPLS all-atom force field on conformational energetics and properties of organic liquids. *J Am Chem Soc* **118:**11225–11236.

Kang J, Chen XL, Wang H, Ji J, Cheng H, Incardona J, Reynolds W, Viviani F, Tabart M, and Rampe D (2005) Discovery of a small molecule activator of the Human Ether-a-go-go-Related Gene (HERG) cardiac K^+ channel. *Mol Pharmacol* **67:**827–836.

Mitcheson JS, Chen J, Lin M, Culberson C, and Sanguinetti MC (2000) A structural basis for drug-induced long QT syndrome. *Proc Natl Acad Sci USA* **97:**12329–12333.

Nose S (1984) A unified formulation of the constant temperature molecular dynamics methods. *J Chem Phys* **81:**511–519.

Parrinello M and Rahman A (1981) Polymorphic transitions in single crystals: a new molecular dynamics method. *J Appl Phys* **52:**7182–7190.

Perry M, Sachse FB, Abbruzzese J, and Sanguinetti MC (2009) PD-118057 contacts the pore helix of hERG1 channels to attenuate inactivation and enhance K^+ conductance. *Proc Natl Acad Sci USA* **106:**20075–20080.

Perry M, Sachse FB, and Sanguinetti MC (2007) Structural basis of action for a human ether-a-go-go-related gene 1 potassium channel activator. *Proc Natl Acad Sci USA* **104:**13827–13832.

Piper DR, Varghese A, Sanguinetti MC, and Tristani-Firouzi M (2003) Gating currents associated with intramembrane charge displacement in HERG potassium channels. *Proc Natl Acad Sci USA* **100:**10534–10539.

Sanguinetti MC, Jiang C, Curran ME, and Keating MT (1995) A mechanistic link between an inherited and an acquired cardiac arrhythmia: HERG encodes the IKr potassium channel. *Cell* **81:**299–307.

Sanguinetti MC and Mitcheson JS (2005) Predicting drug-hERG channel interactions that cause acquired long QT syndrome. *Trends Pharmacol Sci* **26:**119–124.

Sanguinetti MC and Tristani-Firouzi M (2006) hERG potassium channels and cardiac arrhythmia. *Nature* **440:**463–469.

Schönherr R and Heinemann SH (1996) Molecular determinants for activation and inactivation of HERG, a human inward rectifier potassium channel. *J Physiol* **493:**635–642.

Schreibmayer W, Lester HA, and Dascal N (1994) Voltage clamping of Xenopus laevis oocytes utilizing agarose-cushion electrodes. *Pflugers Arch* **426:**453–458.

Schuster A, Lacinová L, Klugbauer N, Ito H, Birnbaumer L, and Hofmann F (1996) The IVS6 segment of the L-type calcium channel is critical for the action of dihydropyridines and phenylalkylamines. *EMBO J* **15:**2365–2370.

Smith PL, Baukrowitz T, and Yellen G (1996) The inward rectification mechanism of the HERG cardiac potassium channel. *Nature* **379:**833–836.

Stary A, Wacker SJ, Boukharta L, Zachariae U, Karimi-Nejad Y, Aqvist J, Vriend G, and de Groot BL (2010) Toward a consensus model of the HERG potassium channel. *Chem Med Chem* **5:**455–467.

Stefani E and Bezanilla F (1998) Cut-open oocyte voltage-clamp technique. *Methods Enzymol* **293:**300–318.

Stühmer W (1992) Electrophysiological recording from *Xenopus* oocytes. *Methods Enzymol* **207:**319–339.

Tikhonov DB and Zhorov BS (2009) Structural model for dihydropyridine binding to L-type calcium channels. *J Biol Chem* **284:**19006–19017.

Trudeau MC, Warmke JW, Ganetzky B, and Robertson GA (1995) HERG, a human inward rectifier in the voltage-gated potassium channel family. *Science* **269:**92–95.

Witchel HJ, Milnes JT, Mitcheson JS, and Hancox JC (2002) Troubleshooting problems with in vitro screening of drugs for QT interval prolongation using HERG K^+ channels expressed in mammalian cell lines and *Xenopus* oocytes. *J Pharmacol Toxicol Methods* **48:**65–80.

Zachariae U, Giordanetto F, and Leach AG (2009) Side chain flexibilities in the human ether-a-go-go related gene potassium channel (hERG) together with matched-pair binding studies suggest a new binding mode for channel blockers. *J Med Chem* **52:**4266–4276.

Zhou J, Augelli-Szafran CE, Bradley JA, Chen X, Koci BJ, Volberg WA, Sun Z, and Cordes JS (2005) Novel potent human ether-a-go-go-related gene (hERG) potassium channel enhancers and their in vitro antiarrhythmic activity. *Mol Pharmacol* **68:**876–884.

Zou A, Curran ME, Keating MT, and Sanguinetti MC (1997) Single HERG delayed rectifier K^+ channels in *Xenopus* oocytes. *Am J Physiol* **272:**H1309–H1314.

Address correspondence to: Dr. Michael C. Sanguinetti, Nora Eccles Harrison Cardiovascular Research and Training Institute, Department of Physiology, University of Utah, 95 South 2000 East, Salt Lake City, UT 84112. E-mail: sanguinetti@cvrti.utah.edu

Downloaded from molpharm.aspetjournals.org by guest on December 1, 2012

aspet